

EDDense-Net: Fully Dense Encoder Decoder Network for Joint Segmentation of Optic Cup and Disc

Mehwish Mehmood^{1,3}, Khuram Naveed^{1,2,*}, Khurshheed Auragzeb⁴, Haroon Ahmed Khan¹, Musaed Alhussein⁴, and Syed S. Naqvi¹

¹Department of Electrical and Computer Engineering, COMSATS University Islamabad, Islamabad, Pakistan

²Department of Electrical and Computer Engineering, Aarhus University, Aarhus, Denmark

³The School of Electronics, Electrical Engineering and Computer Science, Queen's University of Belfast, Belfast, United Kingdom

⁴Department of Computer Engineering, College of Computer and Information Sciences, King Saud University, Riyadh, Saudi Arabia

*Corresponding author: Khuram Naveed, Email: knaveed@ece.au.dk

Abstract—Glaucoma is an eye disease that causes damage to the optic nerve, which can lead to visual loss and permanent blindness. Early glaucoma detection is therefore critical in order to avoid permanent blindness. The estimation of the cup-to-disc ratio (CDR) during an examination of the optical disc (OD) is used for the diagnosis of glaucoma. In this paper, we present the EDDense-Net segmentation network for the joint segmentation of OC and OD. The encoder and decoder in this network are made up of dense blocks with a grouped convolutional layer in each block, allowing the network to acquire and convey spatial information from the image while simultaneously reducing the network's complexity. To reduce spatial information loss, the optimal number of filters in all convolution layers were utilised. In semantic segmentation, dice pixel classification is employed in the decoder to alleviate the problem of class imbalance. The proposed network was evaluated on two publicly available datasets where it outperformed existing state-of-the-art methods in terms of accuracy and efficiency. For the diagnosis and analysis of glaucoma, this method can be used as a second opinion system to assist medical ophthalmologists.

Index Terms—Optic Disc, Optic Cup, OC and OD Segmentation, Grouped Convolution, Dense Network

I. Introduction

Glaucoma leads to permanent blindness worldwide, accounting for the second-highest number of instances of blindness after cataracts [1]. Glaucoma is a treatable condition that requires early detection to prevent progressive and irreversible loss of vision [2] and is typically classified into two types. One is closed-angle glaucoma and the second is open-angle glaucoma. The first one is caused by an obstruction in the drainage angle due to parts of the iris, which results in the inability to drain the excess fluid and results in increased ocular pressure. Acute ocular pain, redness of the eye, sudden reduced vision, and elevated intra-ocular pressure are indications of closed-angle glaucoma [3]. On the other hand, open-angle glaucoma is caused when the drainage angle is left open between the cornea and iris and has no early symptoms leading to difficulty

in early diagnosis and treatment of this type of glaucoma [4]–[9].

The disease is diagnosed clinically by monitoring the pressure inside the eye over the course of many ophthalmologist examinations, where glaucoma causes the internal pressure to exceed 22 mmHg, when normal ocular pressure is between 12 and 22 mmHg [10]. Ophthalmoscopy (observe the health of optic nerve using dilation of pupil) [11], perimetry test (observe the change in the appearance of color or shape of the optic nerve) [12], gonioscopy (identify changes in angle for drainage of fluid in eye) [13], and pachymetry (examine corneal thickness) [14] are some of the main clinical tests used to diagnose glaucoma [15]. All of the above-mentioned techniques, however, are time-consuming, expensive, and may result in inter-observer variability [16].

Computer-based analysis of the retinal image, however, provides a reliable and effective method for detecting Glaucoma, allowing physicians and professionals to quickly evaluate each retinal image separately [7], [17], [18]. In the computerized scenario, the researchers primarily employ the Optic cup-to-disc ratio as an important sign as opposed to a set of tests performed in the clinical case for the detection of Glaucoma disease. This is due to the fact that glaucoma is caused by the weakening of nerve fibers, which gradually affects the optic nerve, which is responsible for conveying signals from the retina to the brain. Intraocular pressure (IOP), or the increase in fluid pressure within the inner region of the eye, damages the optic nerve. Because the eye is unable to evacuate the surplus fluid, builds up pressure, causing the optic nerve fibers damage and thickening of the layers of retinal nerve fiber layers (RNFL). The result is that the optic cup (OC) becomes larger than the optic disc (OD), a phenomenon named cupping. Cupping or cup-to-disc ratio (CDR), which is the percentage of the OC's perpendicular diameter to the OD's perpendicular diameter, is an important metric for glaucoma diagnosis in computational approaches to

the detection of glaucoma [17]. The most efficient technique to identify glaucoma is to examine the optic nerve head (ONH), which is separated into two regions: the optic disc (OD) and the optic cup (OC) [19], [20].

The traditional computer-aided techniques rely significantly on doctors' and ophthalmologists' knowledge, which results in calibrated measurements and observations based on the shapes and sizes of the optic disc and optic cup that have been recorded over time. Optical nerve fibers of a healthy eye degenerate and widen the cup area as intraocular pressure (IOP) rises. This results in an increase in CDR value, which is considered to be less than 0.6 for healthy eyes and more than 0.6 for eyes with glaucoma [21]. However, relying solely on the cup-to-disc ratio to detect glaucoma is insufficient because some patients may have a large OC myopia [21]. The ISNT rule, which stipulates that the rim thickness is thickest in the inferior area of a normal eye, followed by the nasal, temporal, and larger areas of the rim, is utilized for glaucoma screening since glaucoma causes OC size to rise, resulting in a violation of this criterion [22]. However, the exact segmentation of OC and OD is a critical task that is difficult in many ways. For example, fundus cameras are employed to acquire retinal images, resulting in low resolution, poor contrast, noise, and artifacts in retinal images, introducing bright things (such as exudates) that may seem like high-intensity objects similar to OC and OD. As a result, the required candidates, OC and OD, may be falsely detected. Because of these difficulties, segmenting OC and OD is a difficult task. As a result, before segmenting the fundus image for blood vessels, the images must be pre-processed and unwanted noise and poor contrast must be removed [23]. Due to the presence of blood vessels on the layer beneath the retina, detecting the OC borderline is difficult [24]. Numerous authors have proposed levels of pre and post-processing, as well as segmentation, in order to address all of these flaws [25], [26]. Some studies pre-process the image to detect a region of interest (ROI) nearby OD before using a segmentation algorithm [25], [26]. These extra tasks necessitate expert input and additional time for feature extraction and processing, and accuracy varies from case to case, indicating a reliance on input data.

The use of neural networks, particularly state-of-the-art deep-learning-based computerized detection methods, not only eliminates the requirement for data pre-processing and post-processing [27]–[35]. It also ensures competitive performance for combined OC and OD segmentation [36], [37]. Typically, generative adversarial networks with a large number of parameters are used to achieve high accuracy for combined OC and OD segmentation [37], [38]. However, the large number of parameters makes the inference slower and memory intensive [39]–[41]. In [42], the authors implemented an architecture with substantially less parameters while preserving the accuracy of the network, but performance is still dependent on the OD's precise localization.

In a previous study, a novel Cup Disc Encoder-Decoder Network (CDED-Net) design with reduced complexity for OC and OD segmentation from retinal fundus pictures was proposed [7]. The current study proposes a modified CDED-Net that removes superfluous processing blocks and parameters,

reducing the complexity and total computational cost of the deep-learning model previously utilized to segment the cup and disc from retinal fundus images. The new proposal is free from pre or post-processing due to the efficient encoder-decoder network design. In addition, a more efficient encoder-decoder network is proposed to segment the OC and OD robustly. To achieve this, fewer encoder layers are used, resulting in lower parameters and the preservation of semantic information. On the decoder side, a dense layer is also added. The major involvement of this work includes

- 1) As compared to existing state-of-the-art models, a unique encoder-decoder design is described that reduces computational complexity in the training and testing stages. The number of filters utilised for dense connection between the encoder and decoder sides is optimised in this architecture. Furthermore, this architecture efficiently removes pre or post-processing steps.
- 2) The use of grouped convolution in an intelligently designed encoder reduces the complexity of the design without impacting the performance of OC and OD segmentation. When compared to current state-of-the-art methods, this results in a more robust evaluation of glaucoma with less system complexity.

The layout of the paper is given below. The relevant literature is discussed in Section 2. The approach and network structure for OC and OD segmentation are discussed in Sections 3 and 4, respectively. Section 5 contains the experimental data as well as a comprehensive comparison with state-of-the-art methods, with Section 6 providing a full justification for the proposed method. Lastly, section 7 concludes the argument and brings the research project to a culmination.

II. RELATED WORK

Segmenting the OC and OD in order to determine the precise cup-to-disc ratio is a key step in glaucoma diagnosis. Thresholding, region-based methods, and active contour-based methods are among the OC and OD segmentation methods described in this literature review, which are broadly classified as deep learning-based and image-processing techniques. Thresholding is the primary technique for segmenting a binary image, in which the segmented image is obtained by applying a threshold value [43]–[45]. Various thresholding algorithms, such as adaptive thresholding, have been employed for the segmentation of OC and OD due to their efficacy and ease of implementation [46]. Otsu thresholding is a prominent technique to segment OD and OC that uses the red channel of the RGB picture for OD segmentation and the green channel of the ROI image for OC segmentation. By extracting and adding features, quality-independent segmentation, and intensity value can be computed using a threshold. Another method for segmentation is based on the median, mean, and Otsu thresholding. However, the problem with these methods is that patients' retinal color varies, reducing the effectiveness of such solutions.

The use of an active contour model [47] is also suggested for OD segmentation. The initialization of the contour model improves the efficiency of such a system. The existence

of noise and pathologies in an image, on the other hand, causes this system to become stuck on a local minimum [48]. Similarly, in [49], classification errors were reduced by utilizing an adaptive deformable model that recognizes shape changes and irregularities. Furthermore, utilizing a superpixel classification-based approach [50], the segmentation of the cup and disc has been considered. The disadvantage of this method is that fluctuations in cup size lead to inaccurate cup estimation. To segment OC and OD simple linear iterative clustering (SLIC) is used in the superpixel-based approach for the extraction of superpixels from the image and a classifier is used to distinguish between background, OC, and OD regions.

In [24], the use of intensity-based thresholding and geometric features were recommended for OD segmentation and removal of noisy pixels. In [48] a survey is presented in which a technique based on vessel tracking bending was used to track and observe abrupt alterations in blood vessels, however, thresholding-based methods were not efficient in low-contrast images. A method was suggested in [51] to reduce peripapillary atrophy by combining several techniques to obtain an accurate disc boundary. Some studies employed region-based segmentation methods because regional data is more resistant to changes in contrast and intensity. CAR and CDR were estimated in [52] to develop an upgraded segmentation technique for OC and OD. Furthermore, the histogram of the image's red component was used in [53] to choose a threshold for OD segmentation from the green component.

Despite their utility, these traditional approaches suffer from a variety of artifacts, inadequate lighting, and noise in fundus images. To address these challenges, several pre-processing techniques are performed to produce high-quality retinal pictures, which improves segmentation results significantly. As a result, pre-processing techniques, which aim to remove noise, artifacts, and difficulties with non-uniform lighting in fundus images, have become an important part of the OC and OD segmentation pipeline.

Robust segmentation is achieved using machine learning approaches but at the cost of high computational complexity. In [54], a glaucoma detection technique is proposed, in which image classification utilizing statistical characteristics and K-nearest neighbor is employed. Similarly, automated regression is said to be used to determine the proper OC and OD boundary [55]. An effective and accurate approach of OD localization in images with noise and other lesions was proposed in [56]. Deep learning-based methods, in which complicated features are automatically learned through training, have recently become popular. In [57], a transformation of the original U-Net CNN was provided to segment OC and OD, where the image dimensions of the given image are expanded by going through the contracting and expansive network paths with upsampling layers. This approach produces high-quality OC and OD segmentation with the shortest forecast time. In [58], an ensemble learning architecture for OC and OD segmentation was inspired by a CNN. To design convolutional filter learning architecture, the most relevant points were determined using the entropy sampling method. This approach is appropriate for tiny datasets. The authors of [23] proposed a fully convolutional neural network (FCNN) with upsampling

layers, a VGG-16 encoder, and a decoder to achieve the segmented image.

III. PROPOSED METHODOLOGY

In this paper, we propose the EDDense-Net architecture for efficient OC and OD segmentation from fundus images. Traditional deep learning techniques, which use several convolutional layers followed by pooling operations and may lose local information about some essential pixels, are targeted by the proposed architecture. As a result, detecting OC and OD accurately has become difficult by using traditional deep learning techniques. The aim of this study is to propose a network that maintains a fine balance between network complexity and performance.

A. Overview of Proposed Architecture

The general architecture of the suggested technique is depicted in Figure 1, which depicts the configuration of the encoder-decoder block's deep feature concatenation. EDDense-Net receives the original image as input without using any pre-processing technique in this design. The suggested EDDense-Net makes use of the deep feature to import and aggregate high-frequency information from the relevant layers. With the use of pixel-wise segmentation, EDDense-Net can also recognize vessels from low-quality images and non-uniform light. The proposed method produces a binary image with a representation of '1' for the vessel area as output and '0' for the background.

B. OC and OD Segmentation using EDDense-Net

EDDense-Net is designed to tackle those semantic segmentation issues that are not resolved by traditional deep learning techniques by addressing dense connectivity with the following three key design principles:

- 1) Spatial information loss is reduced by using lesser convolutional and pooling layers.
- 2) Immediate spatial information transfer between the layers is provided by the network using dense concatenation within the dense block.
- 3) The faster convergence of the network is achieved by transferring edge information from the first layers of the encoder to the last layer of the decoder.

The encoder is made up of five dense blocks, each with a group convolutional layer. The decoder has a structure that is similar to the encoder. In most existing systems, basic convolution is utilized with dense layers. The process of utilizing a varying number of convolution filter groups on the same image is known as grouped convolution. The number of kernels in each layer is raised in grouped convolution to achieve more than one convolution pathway and improve performance. Grouped convolution increases the network's expressive capacity without increasing the number of parameters. In the network [59], layers of grouped convolution can be simply created with relatively minimal computational overheads. With grouped convolution, large networks may be created simply by replicating the integrated block of the filter group as many

times as desired. Each filter only convolves on a subset of the feature maps obtained by the filter group, minimizing the number of computations required to obtain output feature maps. In the last layer of the suggested architecture, dice pixel classification was used instead of simple pixel classification, which leverages generalized dice loss to overcome the class imbalance problem in semantic segmentation.

C. EDDense-Net Encoder

As demonstrated in Figure 1, EDDense-Net is a densely connected fully convolutional network that uses a total of 5 dense blocks for both encoder and decoder. The encoder is made up of five dense blocks, each of which has a convolutional layer and a grouped convolutional layer. Each encoder dense block begins with a convolutional layer and concludes with a pooling layer that reduces the feature map's size. As a result, the EDDense-Net encoder applies a continual convolutional operation to the image and the feature map, which then flows through the network in a feed-forward method until the image is represented by small features. The issue with CNN is that the max-pooling operation (after convolution) results in the loss of spatial information. The loss of relevant information is covered by grouped convolution with dense layers in EDDense-Net. The encoder is made up of five dense blocks with five grouped convolution layers and five max-Pooling layers in the proposed architecture. For a 640×640 input image, the final feature map is 20×20 . Table I defines the feature empowerment inside each encoder dense block and demonstrates how the bottleneck layer reduces the depth of the feature map. It also illustrates how the EDDense-Net encoder structure in terms of convolution and pooling. The table also includes information on the number of parameters in the encoder's layers.

D. EDDense-Net Decoder

As illustrated in Figure 1, the decoder in EDDense-Net uses the reverse procedure of the encoder, with each dense block starting with a Max-Unpool layer that is responsible for gradually increasing the size of the feature map. A convolution layer is applied after each unpooling layer, followed by grouped convolution. The outer dense routes begin at the encoder dense block's first convolutional layer and end at the concatenation layer of each decoder dense block. To reduce latency, these outer dense paths provide immediate edge information from encoder to decoder. The EDDense-Net decoder, in particular, receives a 20×20 -pixel input from the encoder and outputs a final feature map of the same size as the input image. The network's complexity is reduced by using grouped convolution in each decoder block. The ReLU and Dice pixel classification layer is used to overcome the class imbalance problem in semantic segmentation at the end of the last layer in the decoder (5th decoder dense block). The layer-wise feature map details for the proposed decoder are shown in Table II.

IV. DATABASES AND PERFORMANCE METRICS

The proposed model and the databases used for its assessment are discussed in this section.

A. Retinal Fundus Image Databases

For performance evaluation of our developed model for the tasks of semantic segmentation (pixel-wise) of both OD and OC, we used two publicly available retinal image databases: DRISHTI-GS [60] and RIMONE [61].

1) *Drishti-GS*: This database comprises 101 retinal images taken at a field of view of 30 degrees with a centered-optical disc and dilated pupils. An expert from Aravind Eye Clinic (Madurai, India) annotated each of these collected images. All of the images were saved in PNG format with no compression and have a common resolution of 2896×1944 . In all images of the DRISHTI-GS1, the average OD and OC borders are shown, which are based on four expert hand labelings.

2) *RIM-ONE*: Researchers can use this retinal dataset, which contains 159 images, to evaluate OD/OC segmentation models. 74 of the 159 retinal images belong to glaucoma-affected eyes, whereas the remaining 85 belong to healthy people. These photographs were taken at three Spanish hospitals and graded by two experts.

B. Performance Metrics

We have used standard evaluation metrics for assessing the performance of our developed model on the publicly available datasets of Drishti-GS and RIM-ONE. We have used the evaluation metrics including dice coefficient (F1 score), Jaccard (O), specificity, sensitivity, overlapping error (E) and balanced accuracy (BA). We aim to evaluate our developed EDDense_Net model for the OC/OD segmentation compared to the graded ground truth from experts. The selected evaluation metrics are as given below:

$$Dice_Coefficient(DC) = \frac{TP + TP}{TP + TP + FP + FN} \quad (1)$$

$$Jaccard(O) = \frac{TP}{FN + FP + TP} \quad (2)$$

$$E = 1 - \frac{Area(S \cap G)}{Area(S \cup G)} \quad (3)$$

$$Sen = \frac{TP}{FN + TP} \quad (4)$$

$$Sp = \frac{TN}{FP + TN} \quad (5)$$

$$BA = \frac{Sen + Sp}{2} \quad (6)$$

False positive, true positive, false negative and true negative are abbreviated as FP, TP, FN, and TN respectively. Also, the specificity and sensitivity are referred to by Sp and Sen respectively.

V. RESULTS

We present our experimental results both graphically and in tabular form in this section. Furthermore, the details of the databases and the evaluation metrics used are also unfolded.

Layer	Name and Size	Filters size	The size of the feature map	Parameter information
The 1st block of convolution	Conv1_1/3x3x3	32	640x640x32	896
	groupedconv_1/3x3x1	32	640x640x32	320
1st Pooling layer	Pool1/2x2	2x2	320x320x32	0
The 2nd block of convolution	Conv2_1/3x3x32	64	320x320x64	18496
	groupedconv_2/3x3x1	64	320x320x64	640
2nd Pooling layer	Pool2_1/2x2	2x2	160x160x64	0
The 3rd block of convolution	Conv3_1_1/3x3x64	128	160x160x128	73856
	groupedconv_3/3x3x1	128	160x160x128	1280
The 3rd Pooling layer	Pool2 ₂ /2x2	2x2	80x80x128	0
The 4th block of convolution	Conv3_1_2/3x3x128	128	80x80x128	147584
	groupedconv_4/3x3x1	128	80x80x128	1280
The 4th Pooling layer	Pool2 ₃ /2x2	2x2	40x40x128	0
The 5th block of convolution	Conv3_1_3/3x3x128	128	40x40x128	147584
	groupedconv_5/3x3x1	128	80x80x128	1280
The 5th Pooling layer	Pool3/2x2	2x2	20x20x128	0

TABLE I: The layer-wise feature map details for the downsampling block of the proposed model

Layer	Name and Size	Filter size	The size of the feature map	Parameter information
5th unpooling layer	decoder3_unpool		40x40x128	0
5th block of convolution	decoder3_conv2_1_3/3x3x128	128	40x40x128	147584
	groupedconv_6/3x3x1	128	40x40x256	1280
4th unpooling layer	decoder2_unpool_3		80x80x128	0
4th block of convolution	decoder3_conv2_1_2/3x3x128	128	80x80x128	147584
	groupedconv_7/3x3x1	128	80x80x128	1280
3rd unpooling layer	decoder2_unpool_2		160x160x128	0
3rd block of convolution	decoder3_conv2_1_1/3x3x128	128	160x160x128	147584
	groupedconv_8/3x3x1	128	160x160x128	1280
2nd unpooling layer	decoder2_unpool_1		320x320x64	0
2nd block of convolution	decoder3_conv2/3x3x64	64	320x320x64	36928
	groupedconv_9/3x3x1	64	320x320x64	640
1st unpooling	decoder1_unpool		640x640x32	0
1st block of convolution	decoder1_conv2/3x3x32	32	320x320x64	9248
	groupedconv_10/3x3x1	32	320x320x64	320

TABLE II: The layer-wise feature map details for the upsampling block of the proposed model

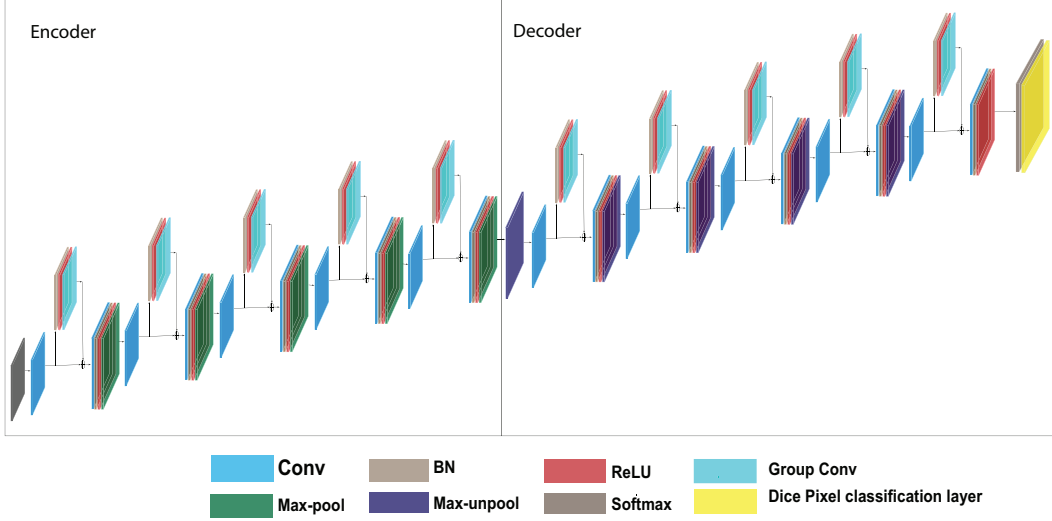


Fig. 1: Proposed Fully Dense Encoder Decoder Network architecture.

A. Performance Metrics

We evaluated our developed model for the segmentation using two databases i.e. Drishti-GS and RIM-ONE and presented the results in Table III and Table IV respectively. Table III indicates that the proposed model achieved the highest dice coefficient (F1 score), Jaccard coefficient (O), and sensitivity for OC detection and comparable results for OD detection on test images from the Drishti-GS dataset. Table IV shows that the proposed model achieved the highest dice coefficient (F1 score) and sensitivity while the second highest Jaccard coefficient (O) for OC detection on test images from the RIM-ONE dataset. It is also evident from this table that the proposed model achieved the highest dice coefficient (F1 score) and sensitivity while the second highest Jaccard coefficient (O) for OD detection on test images from the RIM-ONE dataset. We observed that the proposed EDDense-Net performed much better for OC segmentation than the state-of-the-art methods. For OD segmentation, the proposed EDDense-Net performance is comparable with the state-of-the-art methods. These results proved that the proposed model is robust and reliable and advocates for its use for glaucoma diagnosis.

B. Comparison with state-of-the-art

After the compilation of results, obtained by the proposed design, comparison with state-of-the-art techniques is performed in this section. The visual results of our simulation on the three datasets are shown in Figures 2 and 3 respectively. In each figure, moving from left to right, the first column shows the original images, the second column shows the ground truth images and the third column shows the segmented images.

The segmentation performance of the developed model for the tasks of OD and OC detection using Drishti-GS and RIM-

ONE for the evaluation metrics of error and balance accuracy (Eq. 3 and Eq. 6) is shown in Table V. It is evident from this table that the developed model achieved better BA for both OC and OD detection based on test images from both the considered datasets. Furthermore, it also obtained comparable results for the error metric for both OD and OC detection on the test images from both the datasets.

For visual analysis, the OD and OC segmentation results of the developed model for RIM-ONE and DRISHTI-GS datasets are shown in Figure 3 and Figure 2 respectively.

To evaluate and compare our results with those of state-of-the-art models, we have presented and summarized the results in tabular forms. As given in the tables, the Se, Sp, and Accuracy of our models are 0.8144, 0.9843, and 0.9726 respectively.

In Table III, the results of our proposed model, implemented on the Drishti dataset, are compared with those of state-of-the-art. Se, Sp, and Accuracy of our model are 0.8286, 0.9824, and 0.9689 respectively.

Similarly, results achieved from the implementation of our model on the RIM-ONE dataset are compared in Table IV. From this experiment, dice, Jaccard Se, and Sp of our model are 0.9226, 0.8625, 0.9604, and 0.9978 respectively for OC segmentation and 0.9610, 0.9290, 0.9585, and 0.9987 respectively for OD segmentation.

From the comparisons with state-of-the-art, it is obvious that our proposed model outperformed other existing models with respect to well-known evaluation metric accuracy on three well-known and publicly available datasets.

Figure 2 and Figure 3 represent OD and OC segmentation results on the DRISHTI-GS and RIM-ONE datasets respectively. In [62], Sevastopolsky et al. proposed a method based on the U-Net convolutional network to segment out the OD

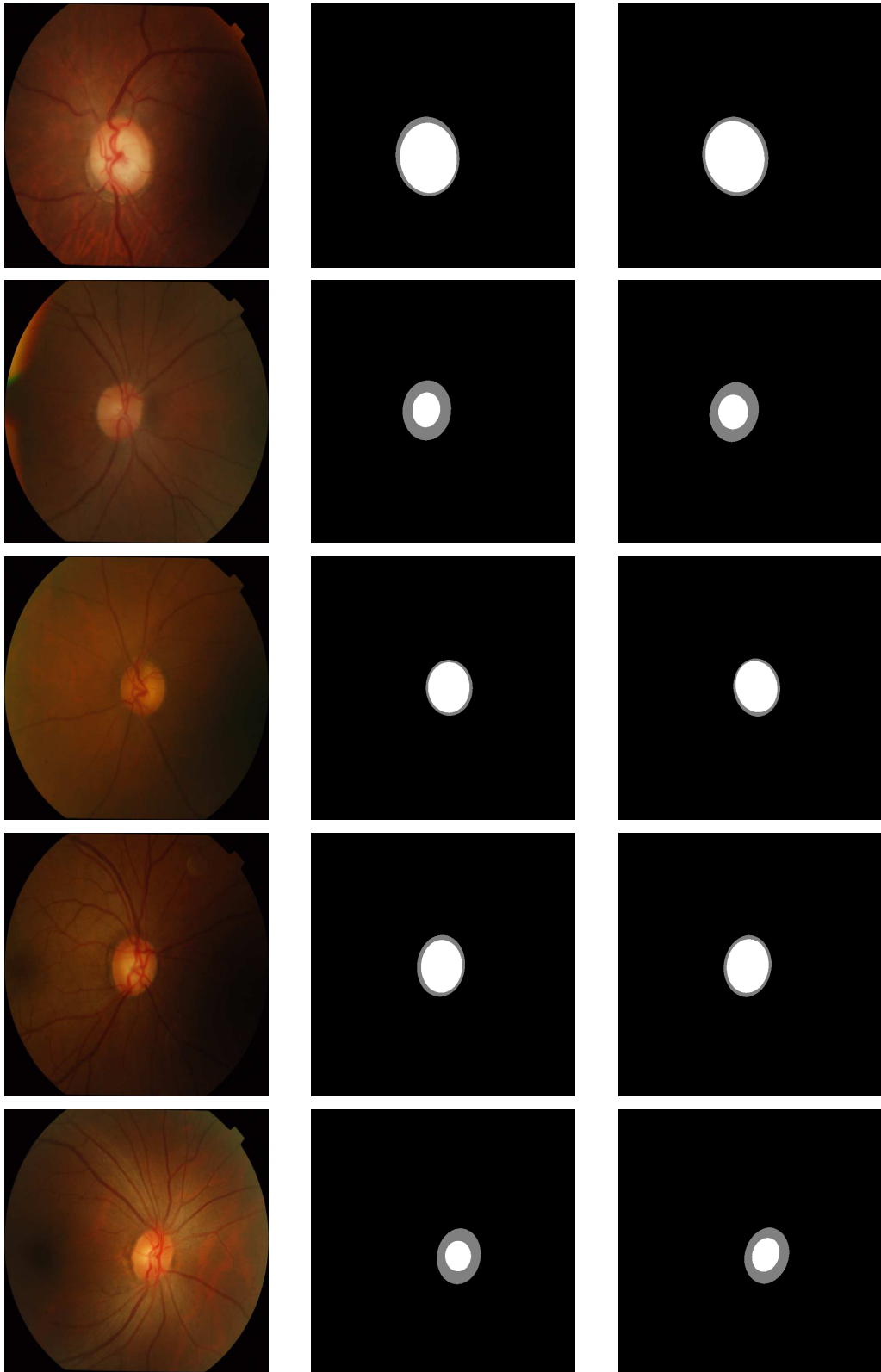


Fig. 2: Visual segmentation results on RIM-ONE dataset delivered by our network.

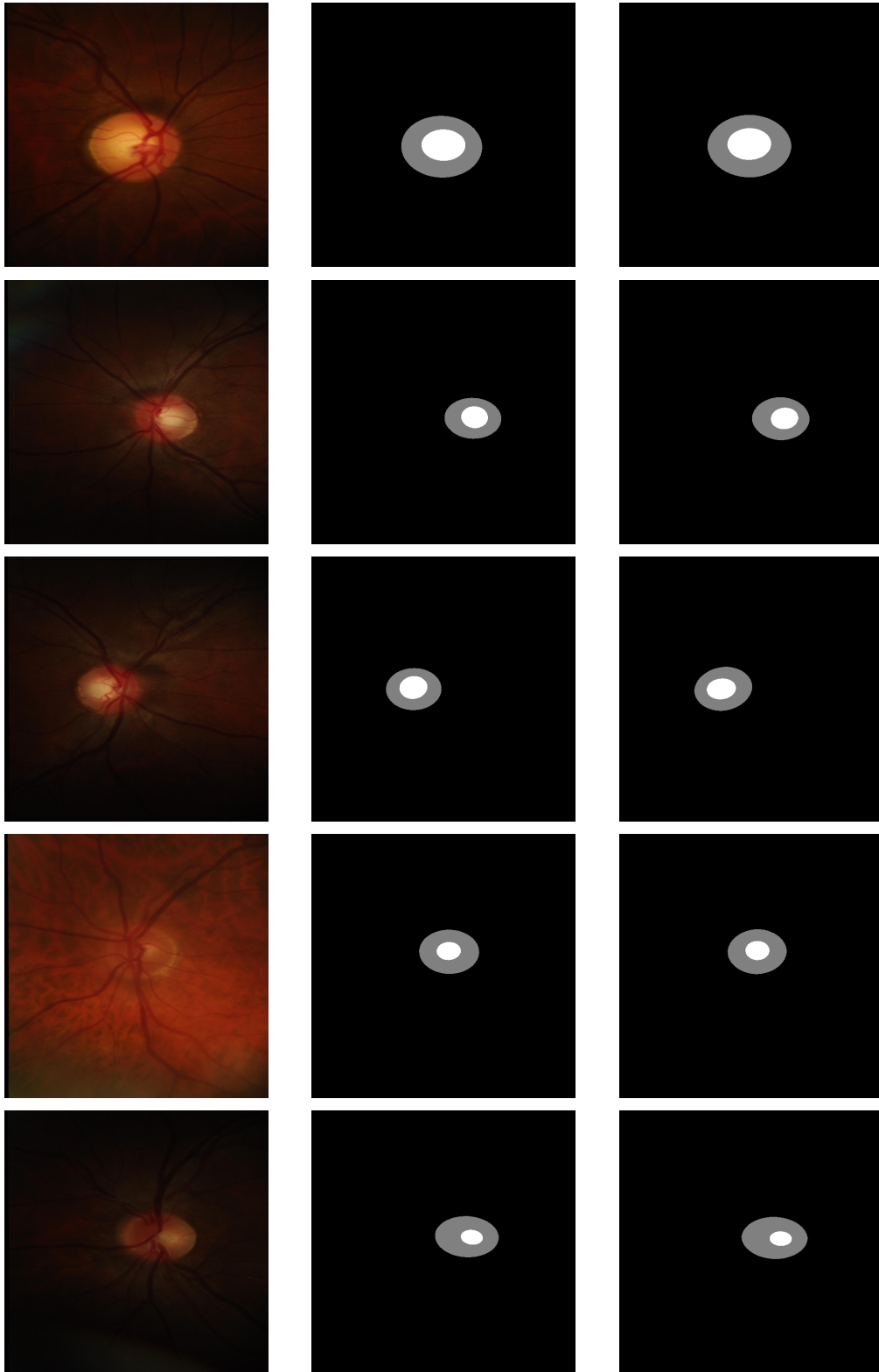


Fig. 3: Visual segmentation results on DRISHTI-GS dataset delivered by our network.

Author	Method	OC				OD			
		DC(F1)	JC(O)	Sensitivity	Specificity	DC(F1)	JC(O)	Sensitivity	Specificity
Sevastopolsky [62]	Modified U-Net CNN	85.21	75.15	84.76	98.81	90.43	83.5	91.56	99.69
Zilly et al. [58]	Ensemble CNN	87.1	85	-	-	97.3	91.4	-	-
Sedai et al. [63]	Regression based method	85	-	-	-	95	-	-	-
Zhou et al. [64]	Locally statistical active contour model	84.7	-	-	-	95.5	-	-	-
Son et al. [65]	GAN Network	86.43	77.48	85.39	99.07	95.27	91.85	97.47	99.77
Chakravarty et al. [66]	RNN based RACE-net	87	-	-	-	97	-	-	-
Fu et al. [67]	M-net	86.18	77.3	88.22	98.62	96.78	93.86	97.11	99.91
Wang et al. [68]	Patch based Output Space Adversarial Learning	85.8	-	-	-	96.5	-	-	-
Gu et al. [69]	Encoder-Decoder CE-Net	88.18	80.06	88.19	99.09	96.42	93.23	97.59	99.9
Xu et al. [70]	U-shaped convolutional neural network	89.2	82.30	-	-	97.8	94.9	-	-
PROPOSED	EDDENSE-NET	92.26	86.25	96.04	99.78	96.10	92.90	95.85	99.87

TABLE III: Performance comparison of the developed model for OD/OC detection of Drishti dataset(%).

Author	Method	OC				OD			
		DC(F1)	JC(O)	Sensitivity	Specificity	DC(F1)	JC(O)	Sensitivity	Specificity
Cheng et al. [71]	Superpixel classification	74.4	73.2	-	-	89.2	82.93	-	-
Aquino et al. [72]	Template-based approach	-	-	-	-	90.1	84.2	-	-
Arnay et al. [73]	Ant colony optimization	-	75.7	-	-	-	-	-	-
Sevastopolsky [62]	Modified U-Net CNN	82	69	75.45	99.76	95	89	95.02	99.73
Zilly et al. [58]	Ensemble CNN	82.4	80.2	-	-	94.2	89	-	-
Zhou et al. [64]	Locally statistical Active contour model	78.5	-	-	-	85.3	-	-	-
Son et al. [65]	GAN Network	82.5	71.65	81.42	99.65	95.32	91.22	94.57	99.87
Fu et al. [67]	M-net	83.48	73	81.46	99.67	95.26	91.14	94.81	99.86
Gu et al. [69]	Encoder-Decoder CE-Net	84.35	74.24	83.52	99.7	95.27	91.15	95.02	99.86
Wang et al. [68]	Patch based Output Space Adversarial Learning	78.7	-	-	-	86.5	-	-	-
Xu et al. [70]	U-shaped convolutional neural network	85.64	75.86	85.15	99.71	95.61	91.72	95.21	99.87
PROPOSED	EDDENSE-NET	90.64	83.18	93.42	99.89	95.84	92.33	95.78	99.84

TABLE IV: Performance comparison of the developed model for the tasks of OD and OC segmentation based on RIM-ONE dataset(%).

and OC. In the case of OD, the achieved dice and Jaccard are 90.43% and 89%. Whereas for OC, it is 82% and 69% on Rim-one. For OC, attained dice and Jaccard are 85% and 75%, and for OD values are 95% and 89% respectively on the Drishti dataset. Zilly et al. proposed an ensemble learning-based CNN model and to reduce the computational complexity, entropy sampling is performed and a framework is designed using boosting for convolutional layers. This algorithm achieved dice and Jaccard of 94.2% and 89% for OD 82.41% and 80.2% for OC on Rim-one. In the case of the Drishti dataset, the acquired dice and Jaccard for OD are 97.3% and 91.4% and for OC; dice and Jaccard are 87.1% and 85% respectively [58]. Cheng et al. presented a superpixel based classification model [71] for the segmentation purpose and the achieved dice and Jaccard are 89.2% and 82.93%, and in the case of OC, 74.4% and 73.2% respectively which is significantly lower than our proposed method. Aquino et al. performed the segmentation of OD using a template-based method [72]. In this method, morphological and edge detection-based techniques were used; followed by CHT which is used to detect the boundary of OD. The attained dice and Jaccard are 90.1% and 84.2% respectively. Ant Colony optimization method was used by [73] for OC segmentation. This method achieved a lower Jaccard value of 75.7% for cup segmentation. Sedai et al. proposed a regression-based method for the segmentation of the OD and OC [63]. Initially, CHT is employed to get the OD and then it is used to estimate the shapes of OD

and OC. For OD, the acquired dice is 95% and for OC the dice is 85%. Zhou et al. presented a locally statistically active contour model with the structure prior (LSACM-SP) approach for joint segmentation [64]. They achieved 95.5% and 84.7% dice values for disc and cup on Drishti and 85.3% and 78.5% values on rim-one. RNN architecture (RACE-net) has achieved 97% and 87% values for dice on disc and cup for Drishti [66]. Wang et al. have proposed a patch-based adversarial network and have achieved 85.8% and 96.5% dice for OC and OD respectively for Drishti and 78.7% and 86.5% cup and disc dice values on rim-one dataset [68]. Their dice value for the cup is much lower than achieved by the proposed architecture. Xu et al. have designed a U-shaped convolutional neural network with multi-scale input and multi-kernel modules (MSMKU) for disc and cup segmentation but their results were lower than the proposed model. Our method has achieved state-of-the values for Jaccard on disc and cup when compared with other methods. Table III and IV 4 also give a comparison of these techniques with the proposed model on both datasets. We have also evaluated our model in terms of sensitivity and specificity. The proposed model achieves state-of-the-art performance on both datasets for disc and cup. It achieves sensitivity and specificity of 93.42%, 99.89% respectively for the OC, and 95.78% and 99.84% for the OD segmentation on RIM-ONE. On Drishti, it achieves sensitivity and specificity of 96.04% and 99.78% for cup and 95.85% and 99.87% for OD segmentation which are higher than other

Methods	Drishti				RIM-ONE			
	OD		OC		OD		OC	
	E	A	E	A	E	A	E	A
Variants proposed in [74]								
Model using residual blocks without depth (ResUnet)	0.089	0.968	0.283	0.926	0.06	0.974	0.321	0.914
Model using DRI blocks without depth (DriUnet)	0.074	0.972	0.286	0.932	0.06	0.974	0.284	0.925
Model using CRF post-processing and DRI blocks (DriUnet CRF)	0.077	0.971	0.27	0.941	0.061	0.974	0.285	0.924
Residual blocks and depth based model (Dept ResUnet)	0.073	0.961	0.268	0.937	0.059	0.974	0.299	0.9353
DRI blocks and Depth based model (Depth DriUnet)	0.068	0.964	0.276	0.936	0.059	0.975	0.31	0.91
DRI blocks and Pseudo-depth based model (PD DriUnet)	0.071	0.972	0.24	0.941	0.058	0.975	0.284	0.92
Proposed								
EDDense-Net	0.0709	0.9585	0.1375	0.9604	0.0691	0.9578	0.1690	0.9342

TABLE V: Segmentation performance of the proposed EDDense-Net on DRISHTI and RIM-ONE dataset using overlapping error (E) and balanced accuracy (BA).

state-of-the-art methods.

For the OD and OC, the performance of the proposed method was compared with a recent work [75] in terms of overlapping error (E) and balance accuracy (A) in Table 5 on the DRISHTI-GS and RIM-ONE datasets. In [75], the authors proposed a fully convolutional network (FCN) for the depth estimation using a pre-training scheme called pseudo-depth reconstruction and a dilated residual inception (DRI) block for multi-scale extraction of features. The guided network was used for OD and OC segmentation using a depth map as a guide and evaluated E and A values for different experiments as shown in Table V. It can be observed from the results that the proposed EDDense-Net outperforms all the variants reported in [75] in terms of E and A measures for the OC segmentation task. Also, the proposed method performs better than all the compared methods on the task of OD segmentation in terms of A, with comparable performance in terms of E. As shown in Table V, our model has achieved state-of-the-art performance with E and A as 0.0709 and 0.9585 for OD and 0.1375 and 0.9604 for OC respectively on Drishti and 0.0691 and 0.9578 for OD as well as 0.1690 and 0.9342 for OC on RIM-ONE.

VI. CONCLUSION

Glaucoma, after cataracts, is the world's second leading cause of permanent blindness. In order to avoid permanent blindness, it is critical to diagnose glaucoma early. We presented an EDDense-Net segmentation network for the joint segmentation of OC and OD in order to proceed with the diagnosis of this disease. The network was able to gather and transmit spatial information from the image by concatenating features in the dense layers. The edge information transfer from encoder layers to decoder layers is used to achieve network convergence quickly. EDDense-Net has four primary design characteristics: EDDense-Net, for starters, uses thick routes for feature empowerment, which aids in the extraction of minor information from the image. Second, to reduce spatial information loss, the optimal number of filters in all convolution layers was utilized. Third, utilizing grouped

convolution reduces the complexity even more. Finally, instead of using simple pixel classification, which uses generalized Dice loss to tackle the class imbalance problem in semantic segmentation, dice pixel classification is employed in the last layer. On two publicly available datasets, the proposed network outperformed existing state-of-the-art approaches in terms of accuracy and efficiency. For the diagnosis and analysis of glaucoma, this method can be utilized as a second opinion system to assist medical ophthalmologists. We will enhance the accuracy of OC and OD segmentation in the future, as well as take into account other retinal illnesses.

REFERENCES

- [1] Y.-C. Tham, X. Li, T. Y. Wong, H. A. Quigley, T. Aung, C.-Y. Cheng, Global prevalence of glaucoma and projections of glaucoma burden through 2040: a systematic review and meta-analysis, *Ophthalmology* 121 (11) (2014) 2081–2090.
- [2] J. L. Wiggs, L. R. Pasquale, Genetics of glaucoma, *Human molecular genetics* 26 (R1) (2017) R21–R27.
- [3] M. I. Rizzo, A. Greco, A. De Virgilio, A. Gallo, L. Taverniti, M. Fusconi, M. Conte, G. Pagliuca, R. Turchetta, M. de Vincentiis, Glaucoma: recent advances in the involvement of autoimmunity, *Immunologic research* 65 (1) (2017) 207–217.
- [4] G. Mowatt, J. M. Burr, J. A. Cook, M. R. Siddiqui, C. Ramsay, C. Fraser, A. Azuara-Blanco, J. J. Deeks, Screening tests for detecting open-angle glaucoma: systematic review and meta-analysis, *Investigative ophthalmology & visual science* 49 (12) (2008) 5373–5385.
- [5] S. S. Naqvi, N. Fatima, T. M. Khan, Z. U. Rehman, M. A. Khan, Automatic optic disk detection and segmentation by variational active contour estimation in retinal fundus images, *Signal, Image and Video Processing* 13 (2019) 1191–1198.
- [6] T. M. Khan, M. Mehmood, S. S. Naqvi, M. F. U. Butt, A region growing and local adaptive thresholding-based optic disc detection, *Plos one* 15 (1) (2020) e0227566.
- [7] M. Tabassum, T. M. Khan, M. Arsalan, S. S. Naqvi, M. Ahmed, H. A. Madni, J. Mirza, Cded-net: Joint segmentation of optic disc and optic cup for glaucoma screening, *IEEE Access* 8 (2020) 102733–102747.
- [8] F. Abdullah, R. Imtiaz, H. A. Madni, H. A. Khan, T. M. Khan, M. A. Khan, S. S. Naqvi, A review on glaucoma disease detection using computerized techniques, *IEEE Access* 9 (2021) 37311–37333.
- [9] S. Iqbal, T. M. Khan, K. Naveed, S. S. Naqvi, S. J. Nawaz, Recent trends and advances in fundus image analysis: A review, *Computers in Biology and Medicine* (2022) 106277.
- [10] H. Öhnel, B. Bengtsson, A. Heijl, Making a correct diagnosis of glaucoma: data from the emgt, *Journal of glaucoma* 28 (10) (2019) 859.
- [11] L. P. Kelly, P. S. Garza, B. B. Bruce, E. B. Graubart, N. J. Newman, V. Biousse, Teaching ophthalmology to medical students (the totems study), *American journal of ophthalmology* 156 (5) (2013) 1056–1061.

- [12] A. M. McKendrick, Recent developments in perimetry: test stimuli and procedures, *Clinical and Experimental Optometry* 88 (2) (2005) 73–80.
- [13] L. M. Sakata, R. Lavanya, D. S. Friedman, H. T. Aung, H. Gao, R. S. Kumar, P. J. Foster, T. Aung, Comparison of gonioscopy and anterior segment ocular coherence tomography in detecting angle closure in different quadrants of the anterior chamber angle, *Ophthalmology* 115 (5) (2008) 769–774.
- [14] S. Schröder, S. Mäurer, T. Eppig, B. Seitz, K. Rubly, A. Langenbacher, Comparison of corneal tomography: repeatability, precision, misalignment, mean elevation, and mean pachymetry, *Current eye research* 43 (6) (2018) 709–716.
- [15] R. Thomas, K. Loibl, R. Parikh, Evaluation of a glaucoma patient, *Indian journal of ophthalmology* 59 (Suppl1) (2011) S43.
- [16] U. Raghavendra, H. Fujita, S. V. Bhandary, A. Gudigar, J. H. Tan, U. R. Acharya, Deep convolution neural network for accurate diagnosis of glaucoma using digital fundus images, *Information Sciences* 441 (2018) 41–49.
- [17] Y. Hagiwara, J. E. W. Koh, J. H. Tan, S. V. Bhandary, A. Laude, E. J. Ciaccio, L. Tong, U. R. Acharya, Computer-aided diagnosis of glaucoma using fundus images: A review, *Computer methods and programs in biomedicine* 165 (2018) 1–12.
- [18] R. Imtiaz, T. M. Khan, S. S. Naqvi, M. Arsalan, S. J. Nawaz, Screening of glaucoma disease from retinal vessel images using semantic segmentation, *Computers & Electrical Engineering* 91 (2021) 107036.
- [19] M. Naveed, A. Ramzan, M. U. Akram, Clinical and technical perspective of glaucoma detection using oct and fundus images: a review, in: 2017 1st International Conference on Next Generation Computing Applications (NextComp), IEEE, 2017, pp. 157–162.
- [20] A. Almazroa, R. Burman, K. Raahemifar, V. Lakshminarayanan, Optic disc and optic cup segmentation methodologies for glaucoma image detection: a survey, *Journal of ophthalmology* 2015 (2015).
- [21] W. Ruengkitpinyo, W. Kongprawechnon, T. Kondo, P. Bunnun, H. Kaneko, Glaucoma screening using rim width based on isnt rule, in: 2015 6th International Conference of Information and Communication Technology for Embedded Systems (IC-ICTES), IEEE, 2015, pp. 1–5.
- [22] N. A. Mohamed, M. A. Zulkifley, W. M. D. W. Zaki, A. Hussain, An automated glaucoma screening system using cup-to-disc ratio via simple linear iterative clustering superpixel approach, *Biomedical Signal Processing and Control* 53 (2019) 101454.
- [23] V. G. Edupuganti, A. Chawla, A. Kale, Automatic optic disk and cup segmentation of fundus images using deep learning, in: 2018 25th IEEE International Conference on Image Processing (ICIP), IEEE, 2018, pp. 2227–2231.
- [24] M. Soorya, A. Issac, M. K. Dutta, An automated and robust image processing algorithm for glaucoma diagnosis from fundus images using novel blood vessel tracking and bend point detection, *International journal of medical informatics* 110 (2018) 52–70.
- [25] B. Al-Bander, B. M. Williams, W. Al-Nuaimy, M. A. Al-Tae, H. Pratt, Y. Zheng, Dense fully convolutional segmentation of the optic disc and cup in colour fundus for glaucoma diagnosis, *Symmetry* 10 (4) (2018) 87.
- [26] P. Qin, L. Wang, H. Lv, Optic disc and cup segmentation based on deep learning, in: 2019 IEEE 3rd Information Technology, Networking, Electronic and Automation Control Conference (ITNEC), IEEE, 2019, pp. 1835–1840.
- [27] T. M. Khan, M. Arsalan, I. Razzak, E. Meijering, Simple and robust depth-wise cascaded network for polyp segmentation, *Engineering Applications of Artificial Intelligence* 121 (2023) 106023.
- [28] S. B. Brahmavar, R. Rajesh, T. Dash, L. Vig, T. T. Verlekar, M. M. Hasan, T. Khan, E. Meijering, A. Srinivasan, Ikd+: Reliable low complexity deep models for retinopathy classification, *arXiv preprint arXiv:2303.02310* (2023).
- [29] T. M. Khan, S. S. Naqvi, A. Robles-Kelly, I. Razzak, Retinal vessel segmentation via a multi-resolution contextual network and adversarial learning, *arXiv preprint arXiv:2304.12856* (2023).
- [30] S. Iqbal, K. Naveed, S. S. Naqvi, A. Naveed, T. M. Khan, Robust retinal blood vessel segmentation using a patch-based statistical adaptive multi-scale line detector, *Digital Signal Processing* (2023) 104075.
- [31] A. Qayyum, M. Mazher, T. Khan, I. Razzak, Semi-supervised 3d-inceptionnet for segmentation and survival prediction of head and neck primary cancers, *Engineering Applications of Artificial Intelligence* 117 (2023) 105590.
- [32] T. M. Khan, M. Arsalan, A. Robles-Kelly, E. Meijering, Mkis-net: a light-weight multi-kernel network for medical image segmentation, *arXiv preprint arXiv:2210.08168* (2022).
- [33] T. M. Khan, S. S. Naqvi, A. Robles-Kelly, E. Meijering, Neural network compression by joint sparsity promotion and redundancy reduction, in: *Neural Information Processing: 29th International Conference, ICONIP 2022, Virtual Event, November 22–26, 2022, Proceedings, Part I*, Springer International Publishing Cham, 2023, pp. 612–623.
- [34] M. Arsalan, T. M. Khan, S. S. Naqvi, M. Nawaz, I. Razzak, Prompt deep light-weight vessel segmentation network (plvs-net), *IEEE/ACM Transactions on Computational Biology and Bioinformatics* 20 (2) (2022) 1363–1371.
- [35] S. Iqbal, S. S. Naqvi, H. A. Khan, A. Saadat, T. M. Khan, G-net light: A lightweight modified google net for retinal vessel segmentation, *Photonics* 9 (12) (2022).
- [36] H. Fu, J. Cheng, Y. Xu, C. Zhang, D. W. K. Wong, J. Liu, X. Cao, Disc-aware ensemble network for glaucoma screening from fundus image, *IEEE transactions on medical imaging* 37 (11) (2018) 2493–2501.
- [37] S. Wang, L. Yu, X. Yang, C.-W. Fu, P.-A. Heng, Patch-based output space adversarial learning for joint optic disc and cup segmentation, *IEEE transactions on medical imaging* 38 (11) (2019) 2485–2495.
- [38] Y. Jiang, N. Tan, T. Peng, Optic disc and cup segmentation based on deep convolutional generative adversarial networks, *IEEE Access* 7 (2019) 64483–64493.
- [39] T. M. Khan, A. Robles-Kelly, S. S. Naqvi, T-net: A resource-constrained tiny convolutional neural network for medical image segmentation, in: *Proceedings of the IEEE/CVF Winter Conference on Applications of Computer Vision*, 2022, pp. 644–653.
- [40] T. M. Khan, A. Robles-Kelly, S. S. Naqvi, Rc-net: A convolutional neural network for retinal vessel segmentation, in: *2021 Digital Image Computing: Techniques and Applications (DICTA)*, IEEE, 2021, pp. 01–07.
- [41] T. M. Khan, A. Robles-Kelly, S. S. Naqvi, A semantically flexible feature fusion network for retinal vessel segmentation, in: *International Conference on Neural Information Processing*, Springer, Cham, 2020, pp. 159–167.
- [42] H. Fu, J. Cheng, Y. Xu, D. W. K. Wong, J. Liu, X. Cao, Joint optic disc and cup segmentation based on multi-label deep network and polar transformation, *IEEE transactions on medical imaging* 37 (7) (2018) 1597–1605.
- [43] T. M. Khan, M. A. Khan, N. U. Rehman, K. Naveed, I. U. Afridi, S. S. Naqvi, I. Raazak, Width-wise vessel bifurcation for improved retinal vessel segmentation, *Biomedical Signal Processing and Control* 71 (2022) 103169.
- [44] A. Khawaja, T. M. Khan, M. A. Khan, J. Nawaz, A multi-scale directional line detector for retinal vessel segmentation, *Sensors* 19 (22) (2019).
- [45] A. Khawaja, T. M. Khan, K. Naveed, S. S. Naqvi, N. U. Rehman, S. J. Nawaz, An improved retinal vessel segmentation framework using frangi filter coupled with the probabilistic patch based denoiser, *IEEE Access* 7 (2019) 164344–164361.
- [46] A. Agarwal, S. Gulia, S. Chaudhary, M. K. Dutta, C. M. Travieso, J. B. Alonso-Hernández, A novel approach to detect glaucoma in retinal fundus images using cup-disk and rim-disk ratio, in: *2015 4th international work conference on bioinspired intelligence (IWOB)*, IEEE, 2015, pp. 139–144.
- [47] J. H. Kumar, A. K. Pediredla, C. S. Seelamantula, Active discs for automated optic disc segmentation, in: *2015 IEEE global conference on signal and information processing (GlobalSIP)*, IEEE, 2015, pp. 225–229.
- [48] N. Thakur, M. Juneja, Survey on segmentation and classification approaches of optic cup and optic disc for diagnosis of glaucoma, *Biomedical Signal Processing and Control* 42 (2018) 162–189.
- [49] M. S. Haleem, L. Han, J. van Hemert, B. Li, A. Fleming, L. R. Pasquale, B. J. Song, A novel adaptive deformable model for automated optic disc and cup segmentation to aid glaucoma diagnosis, *Journal of medical systems* 42 (1) (2018) 1–18.
- [50] J. Cheng, J. Liu, Y. Xu, F. Yin, D. W. K. Wong, N.-M. Tan, D. Tao, C.-Y. Cheng, T. Aung, T. Y. Wong, Superpixel classification based optic disc and optic cup segmentation for glaucoma screening, *IEEE transactions on medical imaging* 32 (6) (2013) 1019–1032.
- [51] J. Cheng, J. Liu, D. W. K. Wong, F. Yin, C. Cheung, M. Baskaran, T. Aung, T. Y. Wong, Automatic optic disc segmentation with peripapillary atrophy elimination, in: *2011 Annual International Conference of the IEEE Engineering in Medicine and Biology Society*, IEEE, 2011, pp. 6224–6227.
- [52] G. D. Joshi, J. Sivaswamy, S. Krishnadas, Optic disc and cup segmentation from monocular color retinal images for glaucoma assessment, *IEEE transactions on medical imaging* 30 (6) (2011) 1192–1205.
- [53] A. Issac, M. Parthasarathi, M. K. Dutta, An adaptive threshold based algorithm for optic disc and cup segmentation in fundus images, in:

- 2015 2nd International Conference on Signal Processing and Integrated Networks (SPIN), IEEE, 2015, pp. 143–147.
- [54] A. Septiarini, D. M. Khairina, A. H. Kridalaksana, H. Hamdani, Automatic glaucoma detection method applying a statistical approach to fundus images, *Healthcare informatics research* 24 (1) (2018) 53.
- [55] S. Sedai, P. K. Roy, D. Mahapatra, R. Garnavi, Segmentation of optic disc and optic cup in retinal fundus images using shape regression, in: 2016 38th Annual International Conference of the IEEE Engineering in Medicine and Biology Society (EMBC), IEEE, 2016, pp. 3260–3264.
- [56] K. Akyol, B. Şen, Ş. Bayır, Automatic detection of optic disc in retinal image by using keypoint detection, texture analysis, and visual dictionary techniques, *Computational and mathematical methods in medicine* 2016 (2016).
- [57] A. Sevastopolsky, Optic disc and cup segmentation methods for glaucoma detection with modification of u-net convolutional neural network, *Pattern Recognition and Image Analysis* 27 (3) (2017) 618–624.
- [58] J. Zilly, J. M. Buhmann, D. Mahapatra, Glaucoma detection using entropy sampling and ensemble learning for automatic optic cup and disc segmentation, *Computerized Medical Imaging and Graphics* 55 (2017) 28–41.
- [59] T. Cohen, M. Welling, Group equivariant convolutional networks, in: *International conference on machine learning*, PMLR, 2016, pp. 2990–2999.
- [60] J. Sivaswamy, S. Krishnadas, A. Chakravarty, G. Joshi, A. S. Tabish, et al., A comprehensive retinal image dataset for the assessment of glaucoma from the optic nerve head analysis, *JSM Biomedical Imaging Data Papers* 2 (1) (2015) 1004.
- [61] F. Fumero, S. Alayón, J. L. Sanchez, J. Sigut, M. Gonzalez-Hernandez, Rim-one: An open retinal image database for optic nerve evaluation, in: 2011 24th international symposium on computer-based medical systems (CBMS), IEEE, 2011, pp. 1–6.
- [62] A. Sevastopolsky, Optic disc and cup segmentation methods for glaucoma detection with modification of u-net convolutional neural network, *Pattern Recognition and Image Analysis* 27 (3) (2017) 618–624.
- [63] S. Sedai, P. K. Roy, D. Mahapatra, R. Garnavi, Segmentation of optic disc and optic cup in retinal fundus images using shape regression, in: 2016 38th Annual International Conference of the IEEE Engineering in Medicine and Biology Society (EMBC), 2016, pp. 3260–3264.
- [64] W. Zhou, Y. Yi, Y. Gao, J. Dai, Optic disc and cup segmentation in retinal images for glaucoma diagnosis by locally statistical active contour model with structure prior, *Computational and Mathematical Methods in Medicine* 2019 (2019).
- [65] J. Son, S. J. Park, K.-H. Jung, Towards accurate segmentation of retinal vessels and the optic disc in fundoscopic images with generative adversarial networks, *Journal of digital imaging* 32 (3) (2019) 499–512.
- [66] A. Chakravarty, J. Sivaswamy, Race-net: A recurrent neural network for biomedical image segmentation, *IEEE Journal of Biomedical and Health Informatics* 23 (3) (2019) 1151–1162.
- [67] H. Fu, J. Cheng, Y. Xu, D. W. K. Wong, J. Liu, X. Cao, Joint optic disc and cup segmentation based on multi-label deep network and polar transformation, *IEEE Transactions on Medical Imaging* 37 (7) (2018) 1597–1605.
- [68] S. Wang, L. Yu, X. Yang, C. Fu, P. Heng, Patch-based output space adversarial learning for joint optic disc and cup segmentation, *IEEE Transactions on Medical Imaging* 38 (11) (2019) 2485–2495.
- [69] Z. Gu, J. Cheng, H. Fu, K. Zhou, H. Hao, Y. Zhao, T. Zhang, S. Gao, J. Liu, Ce-net: Context encoder network for 2d medical image segmentation, *IEEE Transactions on Medical Imaging* 38 (10) (2019) 2281–2292.
- [70] Y.-l. Xu, S. Lu, H.-x. Li, R.-r. Li, Mixed maximum loss design for optic disc and optic cup segmentation with deep learning from imbalanced samples, *Sensors* 19 (20) (2019) 4401.
- [71] J. Cheng, J. Liu, Y. Xu, F. Yin, D. W. K. Wong, N. Tan, D. Tao, C. Cheng, T. Aung, T. Y. Wong, Superpixel classification based optic disc and optic cup segmentation for glaucoma screening, *IEEE Transactions on Medical Imaging* 32 (6) (2013) 1019–1032.
- [72] A. Aquino, M. E. Gegúndez-Arias, D. Marín, Detecting the optic disc boundary in digital fundus images using morphological, edge detection, and feature extraction techniques, *IEEE transactions on medical imaging* 29 (11) (2010) 1860–1869.
- [73] R. Arnay, F. Fumero, J. Sigut, Ant colony optimization-based method for optic cup segmentation in retinal images, *Applied Soft Computing* 52 (2017) 409–417.
- [74] S. M. Shankaranarayana, K. Ram, K. Mitra, M. Sivaprakasam, Fully convolutional networks for monocular retinal depth estimation and optic disc-cup segmentation, *IEEE journal of biomedical and health informatics* (2019).
- [75] S. M. Shankaranarayana, K. Ram, K. Mitra, M. Sivaprakasam, Joint optic disc and cup segmentation using uully convolutional and adversarial networks, in: M. J. Cardoso, T. Arbel, A. Melbourne, H. Bogunovic, P. Moeskops, X. Chen, E. Schwartz, M. Garvin, E. Robinson, E. Trucco, M. Ebner, Y. Xu, A. Makropoulos, A. Desjardin, T. Vercauteren (Eds.), *Fetal, Infant and Ophthalmic Medical Image Analysis*, Springer International Publishing, Cham, 2017, pp. 168–176.